LANGMUIR

pubs.acs.org/Langmuir Article

Development of Solid Lipid Nanoparticle-Loaded Polymeric Hydrogels Containing Antioxidant and Photoprotective Bioactive Compounds of Safflower (*Carthamus tinctorius* L.) for Improved Skin Delivery

Nuur Aanisah, Sulistiawati Sulistiawati, Yulia Yusrini Djabir, Rangga Meidianto Asri, Sumarheni Sumarheni, Lutfi Chabib, Hasyrul Hamzah, and Andi Dian Permana*

Cite This: https://doi.org/10.1021/acs.langmuir.2c02754 Read Online

ACCESS | Metrics & More | Article Recommendations | Supporting Information

ABSTRACT: Safflower (*Carthamus tinctorius* L.) is a potent natural antioxidant because of active compounds such as quercetin (QU) and luteolin (LU). These components prevent damage to the skin caused by free radicals from UV rays. However, due to the poor solubility and transdermal permeation, the effectiveness of the compounds in showing their activity was limited. In this study, we develop solid lipid nanoparticle (SLN)-based hydrogel formulations to enhance the solubility and penetration of two bioactive compounds found in safflower petals extract (SPE). The hot emulsification-ultrasonication method was used to produce SLNs, and to obtain high antioxidant activity, 100% v/v ethanol was used in the extraction procedure. The results showed that this approach could encapsulate >80% of both QU and LU. Moreover, Fourier transform infrared (FTIR), differential scanning calorimetry (DSC), and powder X-ray diffraction (PXRD) spectra indicated that most of the QU and LU were trapped in a lipid matrix and dispersed homogeneously at the molecular level, increasing the solubility. Additionally, SLN-hydrogel composites are able to release two lipophilic bioactive compounds for 24 h, which also demonstrated increased skin retention and penetrability of the QU and LU up to 19-fold. In vitro blood biocompatibility showed that no hemolytic toxicity was observed below 500 μg/mL. Accordingly, the formulation was considered safe for use. Sun protective factor (SPF) test shows a value above 15, showing an excellent promising application as the photoprotective agent to prevent symptoms associated with photoinduced skin aging.

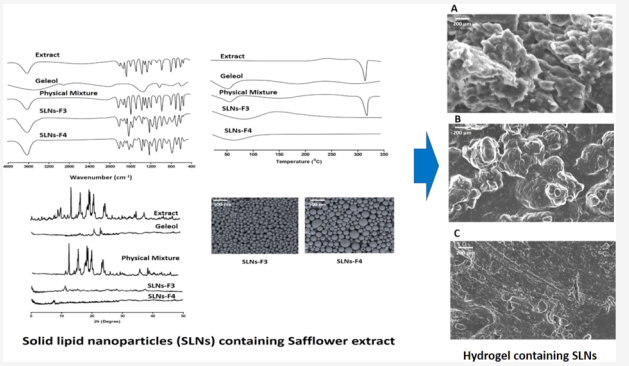

1. INTRODUCTION

Excessive exposure to UV radiation poses risks to skin health, even though ultraviolet rays from the sun may positively mediate vitamin D synthesis[1] and treat several conditions such as psoriasis.[2] The radiation causes acute erythema in subjects with light skin[3] and pigment changes in those with dark skin.[4] These temporary effects may predispose one to the chronic effects of UV radiation, including photoaging, immunosuppression, and photocarcinogenesis.[5−7] There are many endogenous oxidative stress reduction mechanisms present in the human body. Antioxidants are believed to help increase resistance to oxidative stress and reduce indications of photoinduced skin aging. In recent years, natural antioxidants have been an alternative to replace synthetic ones, which are widely suspected of having toxic effects and promoting carcinogenesis. Some well-known antioxidants are polyphenols and flavonoids because they have phenolic OH groups, which allow them to chelate highly redox-active metal ions and enhance their protective effect against oxidative stress.[8,9]

Safflower is a dried stigma of the petals of *Carthamus tinctorius* L. and is classified as a potent natural antioxidant. Through several studies, it has been reported to have antioxidant activity in preventing/treating age-related diseases and oxidative stress such as neuronal[10] and cardiovascular disorders[11,12] as well as cancer.[13,14] This is presumably because it contains chemical compounds such as quercetin (QU)[15,16] and luteolin (LU).[17,18] Due to their potential to contribute a hydrogen atom to the DPPH radical, these bioactive components demonstrated the synergistic impact of a high radical scavenging activity. However, there are a few limitations caused by the original nature, such as low solubility in water

Received: October 10, 2022
Revised: January 13, 2023

resulting in reduced skin permeation abilities.[19−22] In addition, the stratum corneum, which is the outermost layer of the skin, acts as a penetration barrier by blocking the delivery of active ingredients into the skin. This is important because the potential efficacy of QU and LU in preventing cell damage until necrosis mainly occurs in the epidermis.[23,24] Various approaches in terms of drug targeting and carrier systems with different routes of administration were studied to overcome these limitations and achieve more effective therapeutic efficacy.[25−29]

Solid lipid nanoparticles (SLNs) have many features that are advantageous for topical application. It was found that this approach has been a promising carrier for photoprotective agents such as silymarin,[30] tocopherol acetate,[31] and *Aloe vera* powders.[32] SLNs seem to be the main determinant of the extent of lipophilic compounds to penetrate into the epidermal layer of the skin after topical application. Owing to their small size and larger surface area, it is beneficial for targeting skin and upper layers of epidermis to exert its activity in protecting skin tissue from oxidative stress and photoaging. Furthermore, the lipophilic active ingredient trapped between solid lipids offers several benefits. They are physically stable due to a solid matrix, can effectively encapsulate drug molecules, and increase their stability and penetration of the active substance into the epidermal layer of the skin after topical application, resulting in increased bioavailability and greater efficacy.[33−35] In addition, SLNs have an occlusive effect, which can be used to increase the skin's moisture for topical application.[36]

Solid lipid nanoparticles (SLNs) are systems with aqueous colloidal dispersions that have a matrix with solid lipids instead of oil. Several types of solid lipids have been used to prepare SLNs[37−39] but Geleol (glycerol monostearate) is fascinating since even at low concentrations, it is enough to produce SLNs that, after cooling, have a semisolid appearance.[38,39] This occurred due to the lower melting point and composition of Geleol, which contains high amount of monoglycerides that can form hydrogen bonds with water molecules to promote swelling and exhibit a semisolid appearance.[39]

Most sun-care products are semisolid in the form of ointments, gels, cream, or lotion forms and are normally preferred because of their more convenient application. Tursili et al. found that the hydrogel carrier provided stabilization of the microparticle-entrapped sunscreen and increased the skin's retention capacity compared to other carriers.[40] Therefore, hydrogels have received much attention due to their unique advantages: a three-dimensional pore structure that fits the extracellular matrix.[41−43]

However, few studies have examined the skin delivery of bioactive compounds of safflower that has the lipophilic properties as the antioxidant and photoprotective bioactive compounds. Therefore, in our study, we investigated the increased penetration of antioxidant substances of safflower petals extract (SPE), QU, and LU, loaded into a solid lipid nanoparticulate-based hydrogel formulation. The extraction solvent selection was optimized to achieve the maximum phenolic and flavonoid content, and the total phenolic (TPC), flavonoid (TFC), and antioxidant activity were investigated. Subsequently, SPE-loaded SLNs were formulated, optimized, and characterized. Solubility studies, in vitro release and the hemolytic assay were conducted. Finally, considering that antioxidants can efficiently adhere to the skin surface for topical delivery, a hydrogel dosage form was used to apply and hold SPE-loaded SLNs on the skin for protection against UV radiation.

2. EXPERIMENTAL SECTION

2.1. Materials. Safflower samples were obtained from Bone, South Sulawesi, Indonesia. Geleol (glycerol monostearate) was generously provided by Gattefosse Pvt. Ltd., France. Carbomer, poly(vinyl alcohol) (PVA, 9−10 kDa), Tween 80, and sodium dihydrogen phosphate were purchased from Sigma-Aldrich (Dorset, U.K.). Other chemicals used in this experiment were analytical grade.

2.2. Extraction Process. The extraction process, determination of total phenolic content, determination of total flavonoid content, antioxidant activity determination, and HPLC analysis are shown in Section S2.

2.3. Formulation of SPE-Loaded SLNs. SLNs containing SPE were produced through an emulsification-solvent evaporation method. Several formulas were prepared using various lipid concentrations (Geleol), duration of homogenization, and type of surfactants (Tween 80 and PVA) to determine the effect of these formulation parameters on the physicochemical properties of obtained SPE-loaded SLNs. These various formulation parameters are presented in Table 1.

Table 1. Formulation Parameters Used to Prepare SPE-Loaded SLNs

formulation	geleol (mg)	Tween 80 (%)	PVA (%)
F1	100	1	
F2	150	1	
F3	200	1	
F4	250	1	
F5	100		1
F6	150		1
F7	200		1
F8	250		1
F9	100	2	
F10	150	2	
F11	200	2	
F12	250	2	
F13	100		2
F14	150		2
F15	200		2
F16	250		2

In this study, 100 mg of SPE and Geleol, which were accurately weighed according to Table 1 were dissolved in 15 mL of chloroform/methanol mixture (1:1 v/v). The organic phase was slowly poured into the aqueous phase containing the surfactant and processed with a homogenizer Ultra-Turax IKA T18 (IKA, Campinas, Brazil) at 15,000 rpm for 10 min for the F1−F8 formulations and for 20 min for the F9−F16 formulations. Afterward, the organic solvent was removed by stirring for 4 h at room temperature in a fume hood.

2.4. Characterization of SLNs. *2.4.1. Particle Size, PDI, and ζ Potential.* The assessment of mean particle size, polydispersity index (PDI), and ζ potential of the SPE-loaded SLNs was conducted by dynamic light scattering at 90° scattering angle using a Malvern Zeta Sizer (Malvern Instruments Ltd., U.K.), at 25 °C. Specifically, *Z*-average (*d*, nm) with intensity (%) was used to represent the particle size. Before the measurements, the SLNs were diluted with distilled water.

2.4.2. Encapsulation Efficiency. The encapsulation efficiency (EE) was determined by measuring the free drug concentration with the centrifugation method. Dispersion SPE-loaded SLN was centrifuged in a high-speed centrifuge at 14,800*g* for 60 min at 4 °C. Then, the supernatant as the free drug concentration was determined using the previously described HPLC method. The percentage of EE was calculated according to the following equation[44,45]

https://doi.org/10.1021/acs.langmuir.2c02754
Langmuir XXXX, XXX, XXX−XXX

$$\%EE = \frac{a - b}{a} \times 100\% \quad (1)$$

where a and b are the amounts of total SPE-loaded SLN used in the formulation and free drug in the supernatant, respectively; their units are μg/mL.

2.4.3. Fourier Transform Infrared (FTIR) Study. SLN formulation was subjected to an FTIR (Fourier transform infrared) Spectrometer Accutrac FT/IR-4100 Series (Jasco, Essex, U.K.) connected to Diamond MIRacle ATR over a wavenumber range of 4000−400 cm^{-1}.

2.4.4. Differential Scanning Calorimetry (DSC). The DSC analysis was carried out using TA Instruments DSC Q100 (TA Instruments, New Castle, Delaware) to obtain thermograms of SPE, blank SLN, and SPE-loaded SLNs. The specific amounts of each sample were heated in an aluminum pan at a heating rate of 10 °C/min from 25 to 280 °C under a nitrogen atmosphere that was purged at a flow rate of 10 mL/min. The results obtained from the DSC analysis were analyzed using TA Instruments Universal Analysis, version 4.5A.

2.4.5. Powder X-ray diffraction (PXRD). Crystalline characteristics of the SLN formulation were assessed through PXRD-X Miniflex (Rigaku Corporation, Tokyo, Japan). Studies were carried out on the samples by exposing them to Ni-filtered radiation, Cu Kβ (15 mA, 30 kV).[46]

2.4.6. Scanning Electron Microscopy. Morphological examination of SPE-loaded SLN was examined using a scanning electron microscope (SEM) (JEM-1400Plus, Tokyo, Japan). Initially, 100 μL of SLNs were air-dried and coated with gold under vacuum sputter. The analysis was carried out at 15 kV.

2.4.7. Solubility Analysis. The saturated solubility analysis of quercetin (QU) and luteolin (LU) in SPE and SPE-loaded SLNs was performed in 20 mL of water or *n*-octanol in a closed glass vial at room temperature. The blend was mixed under stirring at 500 rpm for 1 h. Afterward, the blend was centrifuged at 2800*g* for 15 min. Subsequently, the supernatant was obtained and analyzed for solubility after appropriate dilution using HPLC analysis.[46]

2.4.8. In Vitro Hemolytic Assay. In vitro hemolytic activity studies were carried out to determine the safety and biocompatibility of SLN formulations loaded with SPE. Wistar rat's erythrocyte samples were separated from plasma using centrifugation at 2000 rpm (20 min). Next, the erythrocytes were washed with PBS three times, mixed using a vortex mixer, and centrifugated for 10 min at 2000 rpm. Then, the washed erythrocytes were resuspended with PBS until they reached a concentration of 10% v/v. Afterward, 100 μL of tested samples were mixed with 900 μL of erythrocytes. The mixture was then incubated for 1 h at 37 °C, centrifuged for 10 min at 7000 rpm, and the absorbance of the supernatant was detected using a UV−vis spectrophotometer (Shimadzu Co., Ltd., Tokyo, Japan) at 540 nm. As positive and negative controls, PBS and water were also measured, respectively. The percentage of hemolytic activity was calculated through the equation below[47,48]

$$\text{hemolysis } (\%) = \left(\frac{\text{Abs}_{\text{test sample}} - \text{Abs}_{\text{negative control}}}{\text{Abs}_{\text{test sample}} - \text{Abs}_{\text{negative control}}} \right) \times 100\% \quad (2)$$

2.4.9. Stability Study. Dispersion of SPE-loaded SLN was filled into sealed glass vials and stored in conditional room temperature (25 ± 2 °C/60 ± 5% relative humidity) for 1 month. Every week, the formulations of SPE-loaded SLN were assessed in terms of particle size.

2.4.10. In Vitro Release Study Using Mathematical Modeling. In vitro release studies were conducted by the dialysis membrane diffusion technique. Briefly, the dispersion was sealed into Spectra-Por, a 12,000−14,000 MWCO dialysis membrane bag (Spectrum Medical Industries, Los Angeles, CA). To achieve sink condition during the release study, PBS (pH 7.4) containing 1% Tween 80 was used as a medium. The study was carried out at 37 °C in an orbital shaker (100 rpm). Furthermore, at each interval time, 1 mL of the medium was collected from the PBS and replaced with the same volume of fresh PBS. Samples were filtered and quantified by the HPLC methodology described in Section S1.6.

To find out the drug release model from the manufactured dosage form, the percentage of drug released was then applied in various mathematical models as follows

Zero order:

$$Q_t = Q_0 + K_0 t \quad (3)$$

First order:

$$\ln Q_t = \ln Q_0 + K_1 t \quad (4)$$

Higuchi:

$$Q_t = K_H \sqrt{t} \quad (5)$$

Korsmeyer−Peppas:

$$Q_t = K_t n \quad (6)$$

Hixson−Crowell:

$$Q_0^{1/3} - Q_t^{1/3} = K_s t \quad (7)$$

where Q_t (%) represents the amount of compound released at time t, Q_0 represents the initial amount of Q_t, t represents the time, n represents the diffusion release exponent, K_0, K_1, K_H, K_t, and K_s represent the release coefficients according to relevant kinetic models.

2.5. Preparation of Hydrogel Containing SLNs. To prepare an SLN hydrogel, Carbomer 940 (1% w/w) and glycerol (10% w/w) were mixed in distilled water and hydrated at room temperature overnight. The dispersion was neutralized by adding triethanolamine (1% w/w), producing a clear hydrogel. Meanwhile, the prepared SPE-loaded SLNs (1% w/w) were incorporated into the hydrogel and mixed evenly at 1000 rpm using a homogenizer. The blank hydrogel was prepared as before but without SPE being loaded into the SLNs.

2.6. Evaluation of Hydrogel. *2.6.1. Drug Uniformity Content and pH.* Briefly, 0.5 g of SLN-based hydrogel was dispersed in 5 mL of methanol and then sonicated for 30 min in a sonicator bath. Following this, the mixture was centrifuged for 15 min at 7000 rpm, and the concentration of bioactive compounds was analyzed using HPLC. Meanwhile, the apparent pH value of the hydrogel formulation was measured using a pH meter under 25 ± 1 °C.

2.6.2. Spreadability. The spreadability was determined by observing the spreading diameter of 0.5 g of hydrogel after being tied up with a standardized weight of 500 g on the upper plate for 5 min.

2.6.3. In Vitro Skin Occlusivity Evaluation. The in vitro occlusion test was conducted according to the De Vringer method with slight modification.[49] Briefly, the first 100 mL beaker was filled with 50 mL of water and covered with Whatman filter paper (Whatman number 6, cutoff size: 3 μm, USA). Furthermore, 250 mg of SPE-loaded SLN hydrogel was spread on the surface of the filter paper and stored at 32 ± 0.5 °C for 48 h (skin temperature). To calculate water loss from evaporation, samples were weighed at 0, 6, 24, and 48 h. Furthermore, for reference, the measuring cup was covered with a filter paper but without the application of the hydrogel. The occlusivity (F_0) was calculated as

$$F_0 = \frac{W_0 - W_1}{W_0} \times 100 \quad (8)$$

where W_0 is the amount of water loss of the reference and W_1 is the amount of water loss of the formulation group.

2.6.4. Ex Vivo Bioadhesive Strength. The bioadhesive strength of the blank (negative control) and SPE-loaded SLN hydrogel formed (positive control) was measured ex vivo using the skin tissue of Wistar rats using the modified balance method. The left side of the double-pan scale was removed, a glass bottle was hung upside down by the string, and another glass bottle was placed under it. Then, the rat skin tissue was washed using normal saline (0.9% NaCl w/v), after which it was followed by immersion in phosphate buffer pH 7.4, which was

https://doi.org/10.1021/acs.langmuir.2c02754
Langmuir XXXX, XXX, XXX−XXX

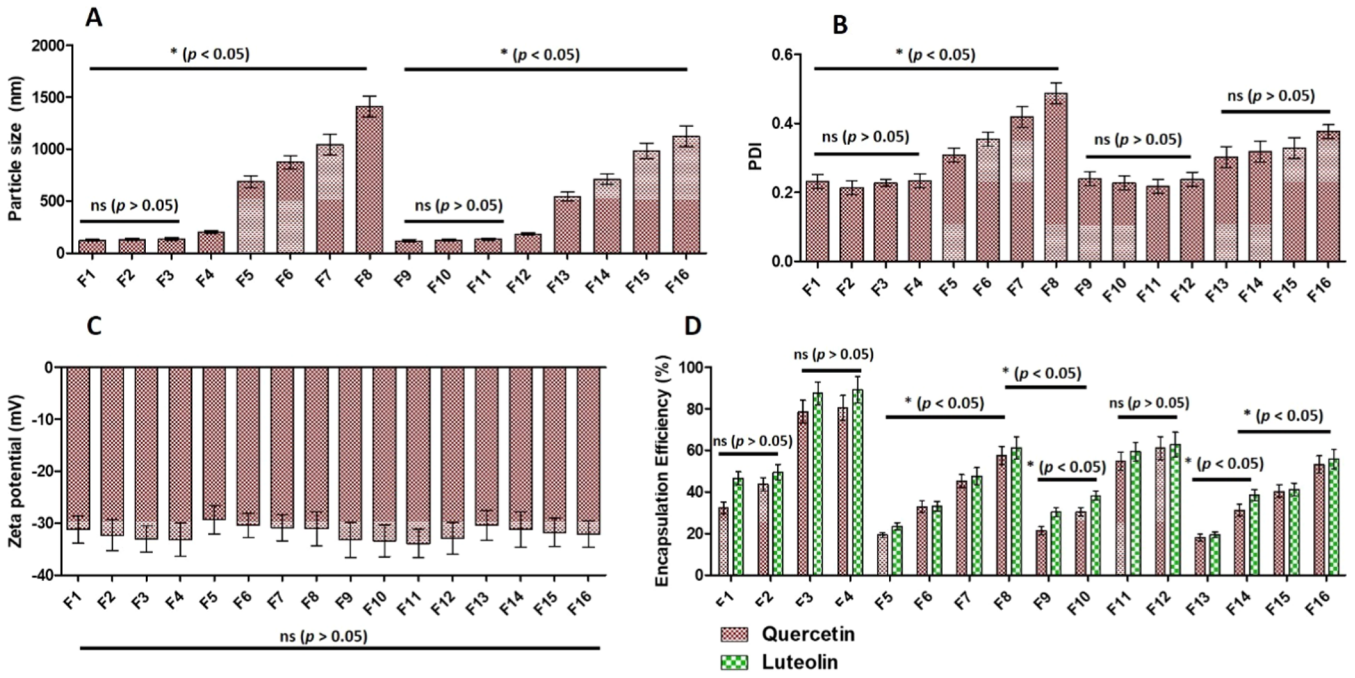

Figure 1. Characterization of nanoparticles. Particle size (A), PDI (B), ζ potential (C) of different SPE-loaded SLN formulations, and encapsulation efficiency of QU and LU (D) of different SPE-loaded SLN formulations (means ± SD, n = 3). ns = nonsignificant, * = significant.

maintained at 37 ± 1 °C for 30 min. Furthermore, the prepared skin tissue was attached to the upper and lower vials, and each 1 g of the hydrogel formulation was pipetted between the skin tissue, which was cut to 4.5 cm^2. The right pan of a double-pan was added with loads every 30 s over the pan to measure the maximum weight required to detach the hydrogel from the skin tissue. The bioadhesive strength was calculated in terms of force per unit area using the following equation[47,48]

$$\text{bioadhesive strength } (N/m^2) = \frac{m \times g \times 0.1}{A} \quad (9)$$

where m is the weight (g) required to remove the formed hydrogel from the rat skin, g is the gravity acceleration (9.8 m/s^2), and A is the surface area of the rat skin (cm^2).

2.6.5. SEM Analysis of the Hydrogel. SEM analysis was carried out to observe the surface morphology of the SLN-based hydrogel. The hydrogel was mounted and sputter-coated with gold after being lyophilized under vacuum. Then, SEM analysis of carried out using a scanning electron microscope (SEM) (JEM-1400Plus, Tokyo, Japan) with an accelerating voltage of 20 kV.

2.6.6. Ex Vivo Skin Permeation and Retention Studies. Ex vivo skin permeation of SPE (negative control) and SPE-loaded SLN formulation (positive control) was conducted using the Franz-type diffusion cells. The abdominal skin of Wistar rats was shaved and mounted on 25 mL of Franz-type diffusion cells after being equilibrated in PBS (pH 7.4) containing 1% w/v Tween 80 as a medium with an effective diffusion area of 4.9 cm^2. The collection of the skin was approved by Ethical Committee, Hasanuddin University, Indonesia. Furthermore, the receptor chamber was filled with 10 mL of diffusion medium, and the cells were maintained at (37 ± 0.5 °C) with stirring at 100 rpm. The 0.5 g of SLN-based hydrogel containing SPE was applied to the skin surface, and 0.5 mL of the sample of the receptor chamber was withdrawn at predetermined time intervals. Afterward, it was immediately replaced with an equivalent volume of fresh medium maintained at 37 ± 0.5 °C. The samples were filtered through an aqueous 0.45 μm membrane filter and analyzed by HPLC to determine the amount of drug permeated from the SLN-based hydrogel.

The drug retained in the skin was also estimated after 24 h following the skin permeation study. The skin was removed and cut into small pieces using scissors, and the pieces were washed three times with distilled water to remove any excess formulations. It was subjected to bath sonication for 6 h to extract the drug from the skin. The samples were centrifuged at 2800g for 15 min, and the supernatant was collected and subjected to HPLC for analysis.

2.6.7. Antioxidant Activity and Sun Protective Factor (SPF) of Optimized Formulation. The antioxidant activity of optimized hydrogel SPE-loaded SLNs was investigated using the previously described method for SPE. We determined the in vitro SPF of SPE using the UV−visible spectrophotometric method. A quantitative solution with the range concentration of 0.1−1 mg/mL was prepared. The SPF value was determined by calculating the absorption of each solution at a wavelength of 290−320 nm with an interval of 5 nm. SPF values were calculated as follows

$$\text{SPF} = \text{CF} \times \sum \frac{320\text{ nm}}{290\text{ nm}} EE_\lambda \times I_\lambda \times \text{Abs}_\lambda \quad (10)$$

where CF (correction factor) is 10 (constant), EE_λ is the erythema effect spectrum, I_λ is the sun intensity spectrum, and Abs is the absorbance of the analyzed sunscreen product.

2.6.8. Statistical Analysis. Quantitative data were presented as mean ± standard deviation (SD) for three replicates. GraphPad Prism version 6 (GraphPad Software) was used to perform statistical analysis of the data obtained, and significant differences were expressed in p values < 0.05.

3. RESULTS AND DISCUSSION

This study was conducted to study the antioxidant potential of SPE-loaded SLN in topical drug delivery. The results of the extraction process, determination of total phenolic content, determination of total flavonoid content, antioxidant activity determination and HPLC analysis are depicted in Section S3. To enhance the penetration of antioxidant substances of safflower petals extract (SPE) such as QU and LU, SPE-loaded SLN formulations have been proposed in the present paper.

3.1. Solid Lipid Nanoparticle Formulation. The effects of various parameters were studied in optimizing SPE-loaded SLN formulation, such as difference in Geleol concentration, duration of homogenization, and type of surfactants (Tween

https://doi.org/10.1021/acs.langmuir.2c02754
Langmuir XXXX, XXX, XXX−XXX

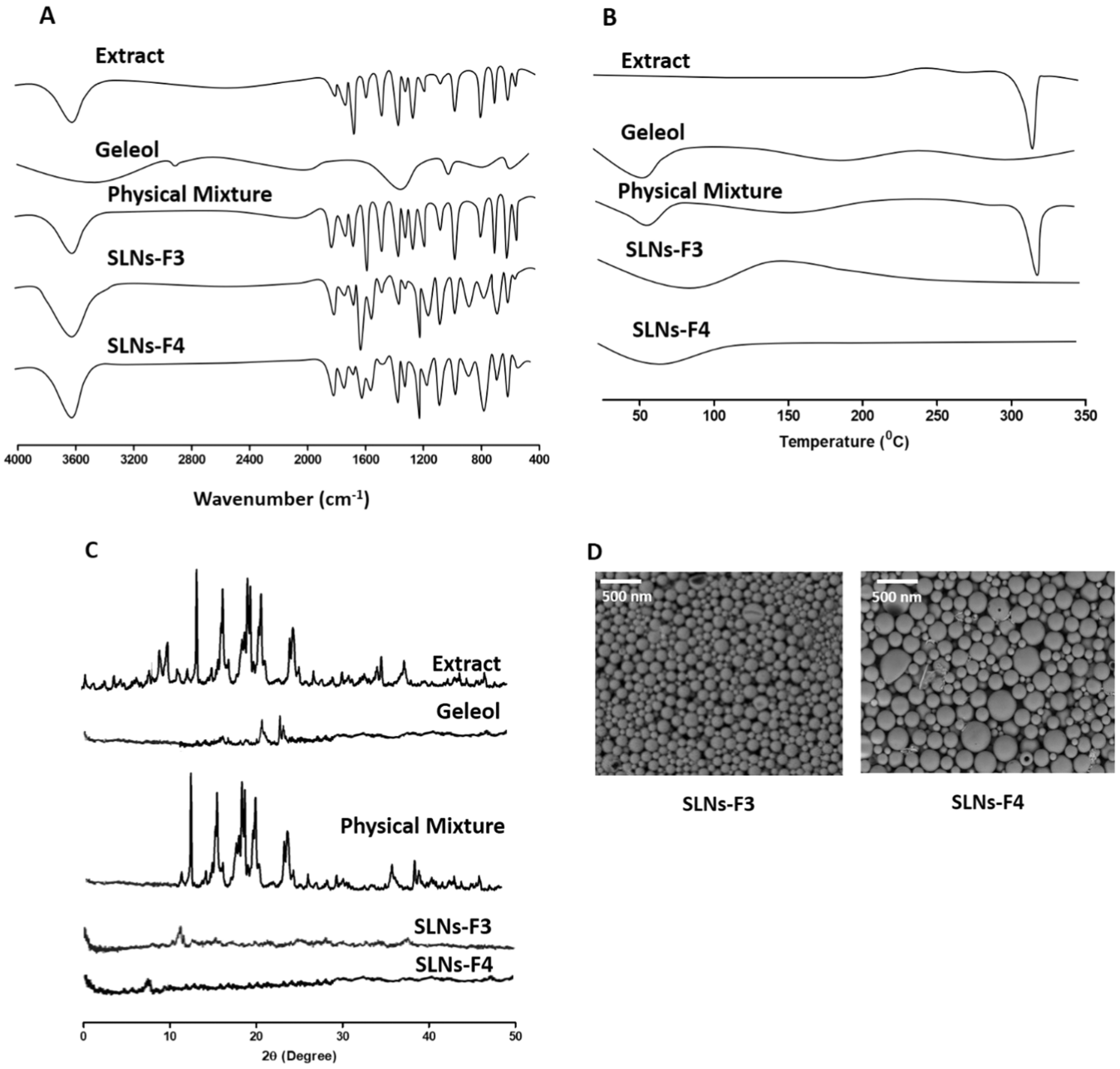

Figure 2. FTIR spectra (A), DSC (B), PXRD diffraction (C) of extract, Geleol, physical mixture, F3 and F4 SPE-loaded SLN formulation, and SEM images of F3 and F4 SPE-loaded SLN formulation (D).

80 and PVA (M_w = 9−10 kDa)) used. Based on previous research, Geleol was selected because it has the lowest melting point of ∼55 °C. This could lead to the lowest viscosity in the medium, resulting in increased homogenization and sonication efficiency to produce smaller particles.[50] Additionally, it showed a semisolid appearance after cooling, even in low concentrations.[39] In the screening of surfactants, Tween 80 and PVA were used because of their nonionic nature.[39,51]

3.2. Characterization of SPE-Loaded SLNs. *3.2.1. Particle size, PDI, ζ Potential, and Encapsulation Efficiency.* As shown in Figure 1A,B, the high concentration of Geleol in the SLN formulation increased the particle size and PDI of SLNs only for the PVA surfactant case. This can be caused by increasing the concentration of Geleol that will increase the viscosity of the dispersion. Therefore, the efficiency of the homogenization and sonication steps in reducing the particle size of the melted lipid droplets was reduced. Meanwhile, the Tween 80 surfactant seemed to produce a more consistent particle size and PDI regardless of Geleol concentration. Regarding the ζ potential measurement, the SLNs varied between −29.33 and −33.91 mV (Figure 1C), indicating electrostatic repulsion between particles to prevent aggregation and stabilize the dispersion of SLNs.[52] All formulations had a negative charge due to the anionic nature of the lipids. The narrow range of ζ potentials could be related to the use of same lipid types with different concentrations. Moreover, the high concentration of Geleol in the SLN formulation also increased the encapsulation efficiency (EE) of QU and LU due to the solubilization of active compounds in the lipid (Figure 1D).

Regarding the type of surfactant utilized in the SLN formulation, Tween 80 (HLB: 15) and PVA (HLB: 18) are

https://doi.org/10.1021/acs.langmuir.2c02754
Langmuir XXXX, XXX, XXX−XXX

both nonionic surfactants. In the same concentration, the surfactant Tween 80 was preferred over PVA because it showed a decrease in the particle size and increased the encapsulation efficiency (EE) of QU and LU. The particle size of SPE-loaded SLNs prepared with higher concentrations of Tween 80 seemed beneficial to slightly reduce the particle size. In addition, it also led to lower the PDI values. Tween 80 has an HLB value in the effective range of 12−16 to produce a stable oil-in-water (O/W) emulsion. A high %EE can also be attributed to the lipophilic nature of QU and LU due to the higher affinity for the lipid matrix. Consequently, it can increase the number of drugs encapsulated in the lipid core.

Increasing the homogenization and sonication time from 10 to 20 min decreased the particle size significantly ($p < 0.05$). The prolonged homogenization and sonication time results in more energy for the nanoparticle dispersion, reducing the size of the SLNs. Considering that the encapsulation efficiency decreased with increasing homogenization time, 10 min was sufficient to obtain the optimal formulation of SPE-loaded SLNs.

According to the results of particle size and encapsulation efficiency of both QU and LU compounds, F3 and F4 were selected to be the optimal formula. The results obtained from F3 and F4 were not statistically significant compared to one another.

3.2.2. FTIR Study. Figure 2A describes the FTIR spectrum of SPE and its formulation in SLNs. The specific functional groups QU and LU in the FTIR spectrum are summarized as follows: SPE: 1150−1500 cm^{-1} (aromatic bonding), 1239 cm^{-1} (−C−O−C bonding), 1367 cm^{-1} (−C−O−H, stretching), 1521 cm^{-1} (C−C═C asymmetric stretching), 1617 cm^{-1} (−C−O stretching of quercetin and C═O vibration of the central heterocyclic ring of luteolin), 1681 cm^{-1} (C═O stretching of the ketone carbonyl), and 3434 cm^{-1} (−OH vibration of the phenolic group of QU and LU). Furthermore, in the spectrum of Geleol, specific peaks were observed at 1215 and 721 cm^{-1}, corresponding to C−H stretching and C−H bending. The results showed that the functional groups characteristic of QU and LU were still recognizable in the FTIR spectrum of the physical mixture and the SPE-loaded SLN formulation. This indicates an adequate entrapment of QU and LU in a lipid matrix and no chemical interaction between the drug and excipients used in the formulation.

3.2.3. DSC Analysis. Several studies regarding the thermal analysis of SLNs used variations of the scanning rate from 1−50 mL/min under nitrogen purge.[53−55] This scan rate level will give different transition temperatures and peak shapes on the DSC melting curve. At high scanning rates, there is no time for the heat to be transmitted from the heating elements of the DSC cell to the sample, resulting in a higher peak transition. Moreover, too high heating rates will give the smooth shape of the melting curve and, as a result, detailed information may get lost. Meanwhile, at a lower scanning rate, it also causes a narrowing of the melting endotherms or crystallization exotherms. A low scan rate (1 °C/min) gives several peaks that are close together. Thus, in the current study, we used 10 °C/min to produce a distinguishable thermal transition.[56]

DSC thermograms of SPE and SPE-loaded SLN are shown in Figure 2B. The profile of the extract showed a sharp endothermic peak at 321 °C, which corresponds to QU and LU melting points that show a highly crystalline nature for these two materials.[57,58] The peak was found at 61 °C in the Geleol thermogram, indicating its melting point. In the thermogram of the physical mixture, all peaks were also observed. However, this peak disappeared in the SPE-loaded SLN formulation. This may indicate complete encapsulation of the two compounds or the transformation to an amorphous state molecularly dispersed in the lipid matrix.[51] The nanoparticles show glass transition characteristics that occurred between 30 and 80 °C, as compared to the extract thermogram. The appearance of the glass transition and the decrease in melting temperature might be attributed to the reduced particle size and increased surface area (Gibbs−Thompson effect).[59]

3.2.4. PXRD and Scanning Electron Microscopy. Figure 2C represents the XRD pattern for the SPE and the optimized formulation, such as F3 and F4. The XRD SPE pattern showed intense peaks at an angle of 2θ 15−30°, and the crystalline nature of the extracted compounds was found. XRD pattern of Geleol showed low peaks between 20 and 25 °C, indicating its low crystallinity. In the physical mixture diffractogram, all peaks were identified. Meanwhile, the peak disappeared in the XRD spectrum of SPE-loaded SLN, which showed amorphous nature that increases solubility. Formulation amorphization revealed that most of the drug was trapped in lipids and dispersed homogeneously at the molecular level, in agreement with the previous DSC results.

SEM images of the optimized SLNs (F3 and F4) are presented in Figure 2D. The results exhibited spherical and homogeneous particles, and the SEM photograph suggested that the SLN possessed a smooth surface. The particle size values shown in the SEM were in close agreement with the size measurements by PSA, which are approximately 135.98 ± 12.09 and 202.36 ± 14.21 nm for F3 and F4, respectively.

3.2.5. Solubility Analysis. The solubilities of QU and LU are essential factors that must be considered in the SLN formulation. In this study, we compared the solubilities of QU and LU from SPE, as well as from formulas F3 and F4 SPE-loaded SLN in water and *n*-octanol solvents. The test results are depicted in Table 2, which shows that the water solubilities of compounds QU and LU (SPE) were observed to be 28.32 ± 2.13 and 17.23 ± 1.61 μg/mL, respectively. Meanwhile, the solubilities of QU and LU (SPE) compounds in *n*-octanol showed a significantly different solubility effect ($p < 0.05$) compared to their solubility in water, namely, 498.56 ± 43.21 and 504.34 ± 47.87 μg/mL for QU and LU, respectively. This also explains the hydrophobic nature of the compound.

Table 2. Solubilities of QU and LU from Safflower Petals Extract (SPE), F3, and F4 of SLN Formulations (Means ± SD, $n = 3$)

compound	samples	aqueous solubility (μg/mL)	*n*-octanol solubility (μg/mL)
quercetin (QU)	SPE	28.32 ± 2.13	498.56 ± 43.21
	SLN-F3	385.43 ± 21.43	509.44 ± 47.03
	SLN-F4	309.41 ± 29.37	503.12 ± 48.38
luteolin (LU)	SPE	17.23 ± 1.61	504.34 ± 47.87
	SLN-F3	358.43 ± 31.98	598.57 ± 54.39
	SLN-F4	299.73 ± 27.46	549.59 ± 51.37

Furthermore, the solubilities of QU and LU of the SPE-loaded SLN formulation showed an increase in the solubilities of QU and LU in water and *n*-octanol. The solubilities of QU and LU of the SPE-loaded SLN formulation in water showed a significant ($p < 0.05$) increase of approximately 12- and 20-fold

https://doi.org/10.1021/acs.langmuir.2c02754
Langmuir XXXX, XXX, XXX−XXX

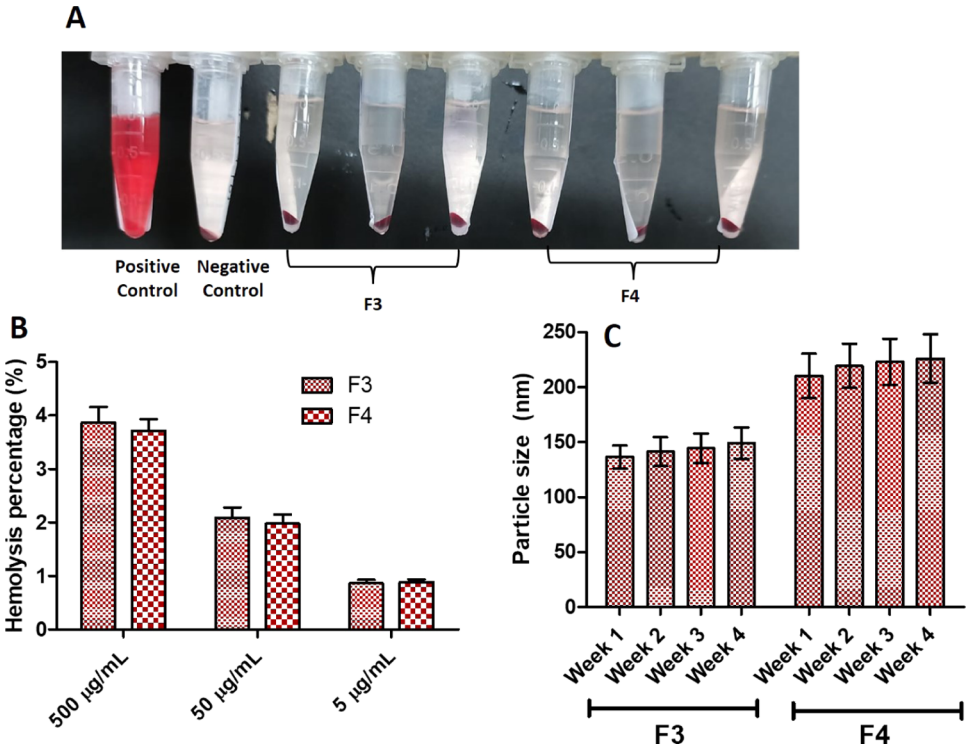

Figure 3. Hemolytic activity test. Image representative (A), hemolysis index value (B), and stability study results of SLNs (C) (means ± SD, n = 3).

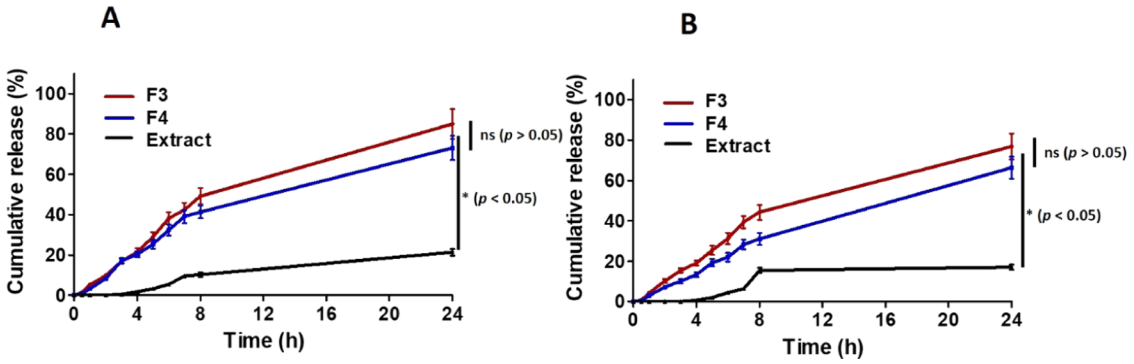

Figure 4. In vitro drug release profile of QU (A) and LU (B) from F3, F4, and Safflower extract (means ± SD, n = 3). ns= nonsignificant, * = significant.

for QU and LU, respectively, compared to the solubility of the compound from SPE in water. A small increase was observed in n-octanol, ∼1.1 times higher than SPE. This significant increase (p < 0.05) of aqueous solubility was due to the heating step of the hot emulsification process, in which the active compounds partitioned from the lipid droplets in the SLN formulation melted into the aqueous phase.[24] Several studies have demonstrated the drug delivery capability of solid lipid nanoparticle systems in increasing solubility for hydrophobic drugs or having low solubility in water.[23,60,61]

3.2.6. In Vitro Hemolytic Assay. In this work, the in vitro hemolysis assay was used to measure the hemocompatibility of SPE-loaded SLNs. The index value considered safe was less than 5%.[62] A hemolytic activity assay was carried out using Wistar rats. From Figure 3A,B, the formulation of SLNs containing SPE showed a hemolysis value of less than 5% at all tested concentrations (5−500 µg/mL) of SPE-loaded SLNs. Therefore, the prepared SPE-loaded SLNs had no hemolytic effect and were considered safe for use at the concentrations tested.

3.2.7. Stability Study. In an attempt to assess the stability of the SLNs, the particle size was observed for 1 month at 25 °C. The result of this study is depicted in Figure 3C, indicating that despite the increase in the particle size, there was no significant difference (p < 0.05) after 1 month storage. Accordingly, it could be concluded that both formulations were physically stable.

3.2.8. In Vitro Drug Release. The cumulative percentage drug release from SPE and optimized SPE-loaded SLN formulations were investigated for 24 h (Figure 4). The release of the active compound from SPE for 24 h was 20.35 ± 1.72 and 17.06 ± 1. 32% for QU and LU. Meanwhile, when SPE was incorporated into SLNs, the release of QU and LU became significantly faster (p < 0.05), reaching 84.98 ± 7.43 and 76.81 ± 6.43% for F3 and 73.14 ± 6.05 and 66.34 ± 5.38% for F4. Combining SLNs and hydrogels will display both

https://doi.org/10.1021/acs.langmuir.2c02754
Langmuir XXXX, XXX, XXX−XXX

component advantages such as the protection and improvement of the solubility of the lipophilic active molecule while improving the drug release. Even though the drug release from SPE-loaded SLN-bearing hydrogel formulations is faster, the sustained drug release for 24 h will still be observed, suggesting their applicability as the carrier to protect the skin from UV rays all day.

Moreover, the percentage of drug dissolution data was fixed in several kinetic models to evaluate the dissolving mechanism and QU and LU from SLN matrices (Table 3). The most suitable release model was selected according to the correlation coefficient value. The results revealed that the release profile of the two compounds from the SLN formulation seemed to follow the Higuchi model ($R > 0.95$). Meanwhile, the SPE-loaded SLNs showed a high correlation for the Higuchi model, where the release of the drug from the formulation was controlled by diffusion through the matrix.

Table 3. Kinetic Models of SPE-Loaded SLNs

	regression coefficient (R^2) values				
formula	zero-order	first-order	Higuchi	Hixson–Crowell	Korsmeyer–Peppas
F3	0.81	0.93	0.98	0.87	0.95
F4	0.84	0.92	0.97	0.83	0.92

3.3. Characterization of SLN Hydrogels. *3.3.1. Drug Uniformity and pH.* To assess the effect of the formulation on the distribution of compounds in the hydrogel formulations, a content uniformity test of the two main chemicals of SPE in the SPE-loaded SLN formulation was carried out. Figure 5A showed that the analyte recovery results at F3 were 97.65 ± 1.32 and 98.56 ± 1.43% for QU and LU, respectively. Meanwhile, the analyte recovery results at F4 were 99.54 ± 1.62 and 98.18 ± 1.58% for QU and LU, respectively. These results indicate that the formulation procedure carried out did not affect the recovery and homogeneity of QU and LU compounds in the hydrogel, so the two formulas produced can be considered to possess good content uniformity. Regarding formulation pH (Figure 5B), the blank hydrogel's pH was 6.74 ± 0.23, while the pH of the charged hydrogel SLNs was in the range of 5.56 ± 0.21 and 5.61 ± 0.19 for F3 and F4, respectively. The pH of the hydrogel was in the normal skin pH range of 5–6. The pH test was important to determine the acidity level of the formulation made to prevent irritation.

3.3.2. Spreadability. SLN-incorporated hydrogels were further evaluated for spreadability to evaluate customer compliance, depicted in Figure 5C, and the dispersion was found to be 56.54 ± 2.87 mm for the blank gel. Meanwhile, the dispersion of the F3 and F4 hydrogels was 55.98 ± 2.71 and 56.01 ± 2.93 mm, respectively. The standard range of a suitable hydrogel formulation is between 50 and 70 mm. Based on F3 and F4, the results of the dispersion test were equally acceptable. Additionally, the incorporation of SPE-loaded SLNs into the hydrogel formulation did not change ($p > 0.05$) the spreadability of the final products.

3.3.3. Skin Occlusivity Evaluation. To assess the ability of the SPE-loaded SLN formulation to maintain its skin hydrating properties after application, an in vitro evaluation of the skin occlusives was carried out. The results of in vitro skin occlusives for 48 h are shown in Figure 5D. Furthermore, F3 and F4 showed an increase in occlusiveness of 59.09 ± 4.31 and 62.43 ± 4.87%, respectively, when the shell occlusive values of the blank gels (38.77 ± 2.78%) were compared with those of the hydrogel SLNs. Better occlusion properties incorporated with SPE-loaded SLNs can be attributed to the dense nature of the lipid components. This prevents the evaporation of water to a greater extent and also to the aqueous phase of the hydrogels. It can increase skin hydration for up to 48 h, allowing drug penetration through the stratum corneum due to the reduction of the corneocyte gap.[63]

3.3.4. Bioadhesive Strength. Flexibility and softness are characteristics of an ideal topical hydrogel, but the ability to withstand pressure damage from external mechanical forces and the ability to stick to the skin for a long time after application are also characteristics that must be met by the hydrogel. Therefore, in this study, a bioadhesive strength test was carried out on the SPE-loaded SLN formula. There are three types of gel tested in this study, namely, blank gel and gel containing F3 and F4. Figure 5E shows the bioadhesive strength of each hydrogel. The results of the three gels showed that the addition of SPE-loaded SLNs into the hydrogel did not change the ability of the gel to adhere to the skin. Then, based on statistical results, no significant difference was observed for each hydrogel made. This particular trend can be attributed to the fact that the anionic hydrophilic polymer used, Carbopol 940, tends to disentangle due to its carboxylic acid groups being partially ionized in solution, which leads to bioadhesion.[67] In addition, Carbopol 940 undergoes cross-linking so that it has a longer contact time on the skin, and hence more available for interpenetration with the superficial epithelial cells.[68]

3.3.5. SEM Analysis of the Hydrogel. Following the observation using SEM, it was found that all hydrogel formulations possessed a rough surface with higher brawl borders. SEM images of all formulations are exhibited in Figure 6. As shown, the SLNs were completely entrapped in the hydrogel matrices. Therefore, this could potentially provide sustained release behavior of the bioactive compounds from Carbopol-based hydrogel formulations.[64] Furthermore, the release of the bioactive compounds could be facilitated through the small pores between the hydrogel network, as shown in Figure 6.

3.3.6. Skin Permeation and Retention Studies. The cumulative amount of QU and LU permeating the skin from SPE, F3, and F4 hydrogels is reported in Figure 7. The results showed that the skin permeation of QU and LU in SPE for 24 h was very small at 1.98 ± 0.17 and 1.19 ± 0.12%, respectively. On the other hand, F3 and F4 SLN-based hydrogel permeations increased significantly ($p < 0.05$). After applying the F3 hydrogel for 24 h, 39.84 ± 3.87 and 37.49 ± 3.09% of the applied QU and LU permeated through the skin, respectively. Meanwhile, QU and LU permeations from hydrogel F4 after 24 h were calculated to be 21.24 ± 2.09 and 19.24 ± 1.72%, respectively. SLNs have been linked to higher levels of penetration due to their direct effect on skin hydration, causing increased water retention in the stratum corneum as a result of film formation from fatty esters that are bound only by van der Waals interactions to the skin surface. These fatty esters forming lipid particles enable the drug to pass through the skin's deep layers.[49,56,65] The skin permeation value of F3 was found to be higher than that of F4 because of the smaller particle size. In the skin permeation study using a Franz diffusion cell, the rate depends on various factors, such as the particle size. Smaller particle sizes could potentially result in more drug permeation. However, there is still ongoing

https://doi.org/10.1021/acs.langmuir.2c02754
Langmuir XXXX, XXX, XXX–XXX

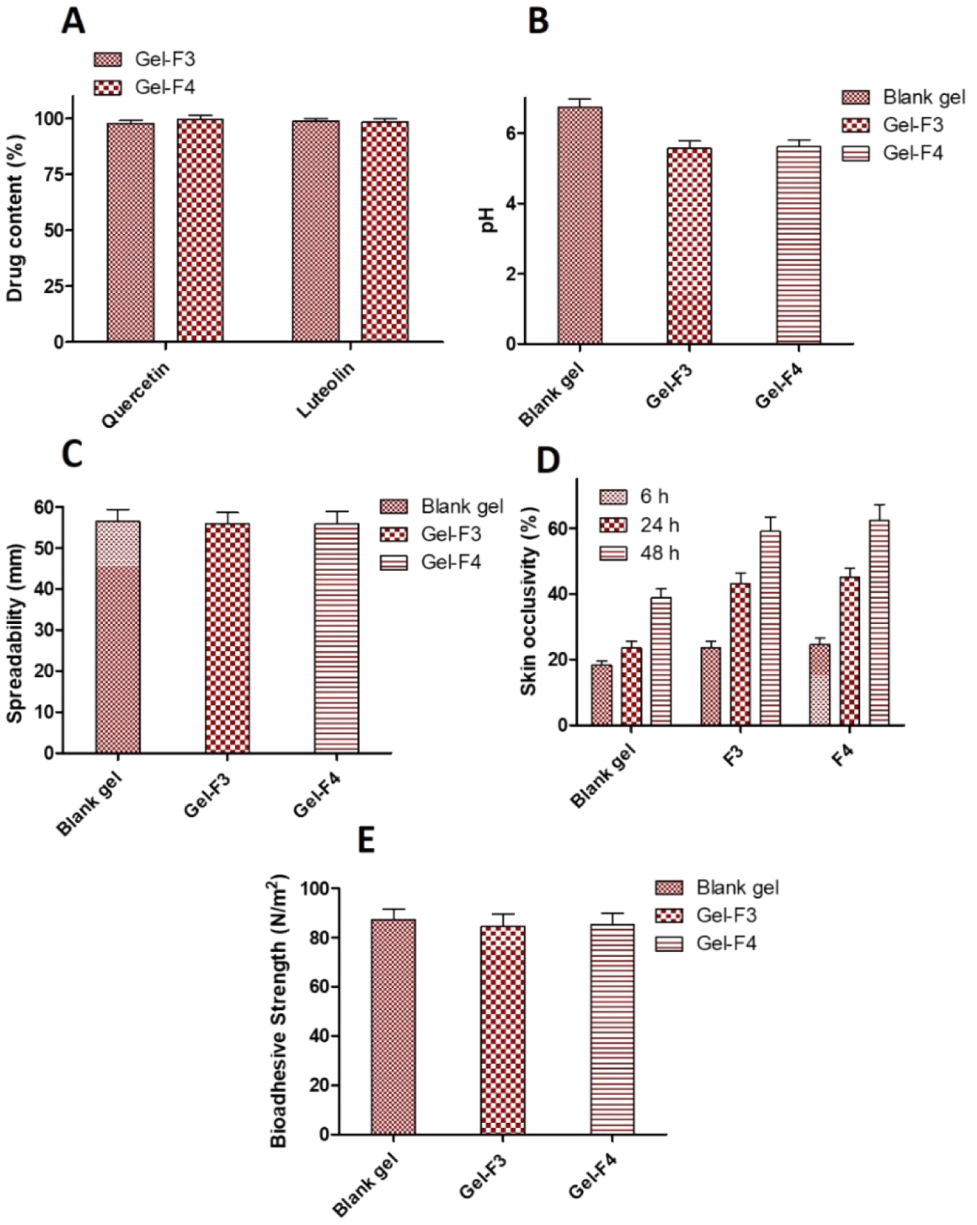

Figure 5. Drug uniformity content (A), pH (B), spreadability (C), in vitro skin occlusivity (D), and bioadhesive strength (E) of hydrogel formulation in comparison with blank hydrogel (means ± SD, n = 3).

discussion regarding the precise number representing the maximum diameter of nanoparticles that can be penetrated through the skin. Several studies have shown that the smaller particle size indicates higher and faster skin penetration. Later, Lademann found that 300−600 nm particles were still able to penetrate the follicle on massage as a consequence of the spacing between the scales on the hair and suggested that the movement of the hair serves as a directed pump to push the particles into the follicles.[66]

These data also show good drug retention in the epidermal layer. Since the lipoperoxidation inhibition process occurs mainly when the active component passes through the epidermis, skin drug retention is a significant factor impacting the efficacy of antiaging therapies. Drug retention increased when SPEs were incorporated into SLNs (Figure 8A−C). Higher SPE lipophilicity and potential effects of SLN on the skin are associated with a 19-fold increase. Regarding drug retention, F4 was greater than F3 due to the bigger particle size.

The retention profiles of QU and LU can be attributed to the occlusive properties of the previously described SLN, where occlusives can increase skin permeability and hydration. In addition, drug accumulation in the upper skin layer can also occur, resulting in decreased drug flux, and the drug residence time in the skin can be extended by creating a reservoir. Thus, these antioxidant agents can provide longer-lasting protection.

3.4. Antioxidant Activity and Sun Protective Factor (SPF) of Optimized Formulation. The evaluation of antioxidant activities of F3 and F4 hydrogels against DPPH and lipid peroxidation are shown in Figure 8D. IC50 values against DPPH were found to be 36.65 ± 2.86 μg/mL and 37.09 ± 3.02 μg/mL for F3 and F4, respectively. Meanwhile, IC50 values in inhibition of lipid peroxidation were 49.65 ± 3.32 μg/mL for F3 and 51.23 ± 4.98 μg/mL for F4. Statistical analysis showed that the SPE-loaded SLN formulas F3 and F4

https://doi.org/10.1021/acs.langmuir.2c02754
Langmuir XXXX, XXX, XXX−XXX

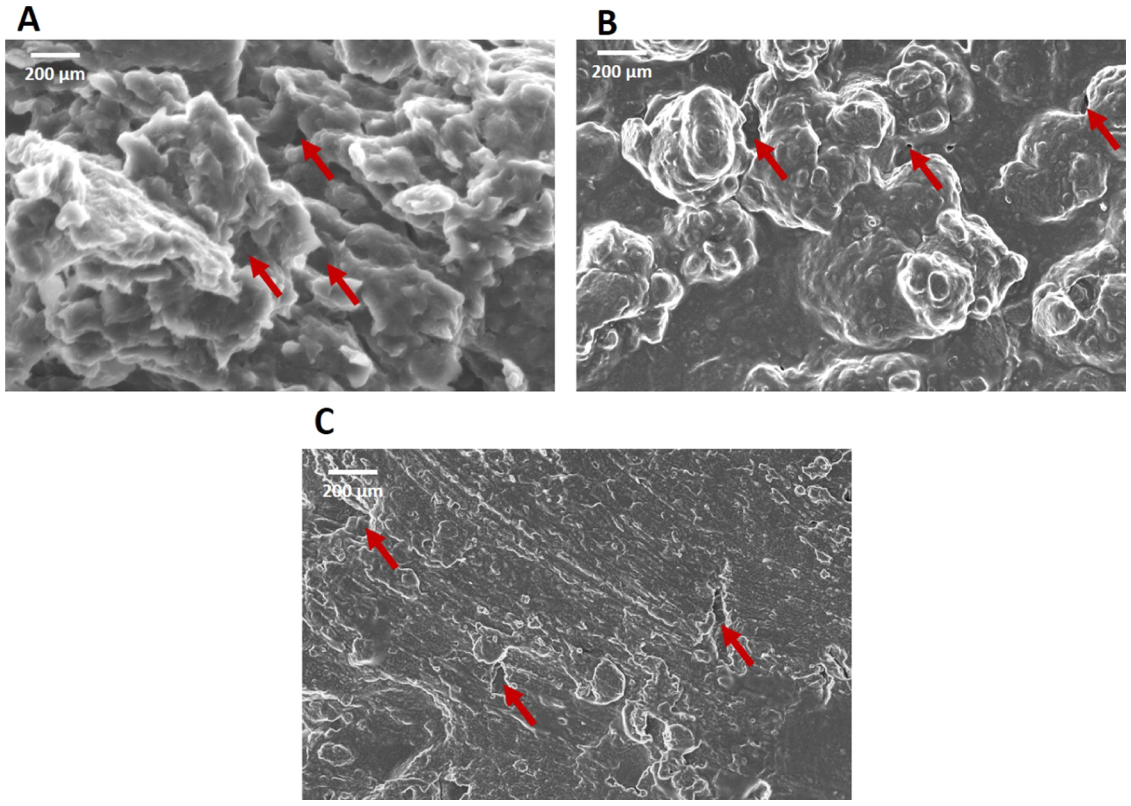

Figure 6. Morphology of hydrogels containing F3 (A), F4 (B), and extract (C) analyzed by SEM. The pores of the hydrogels are pointed by red arrows.

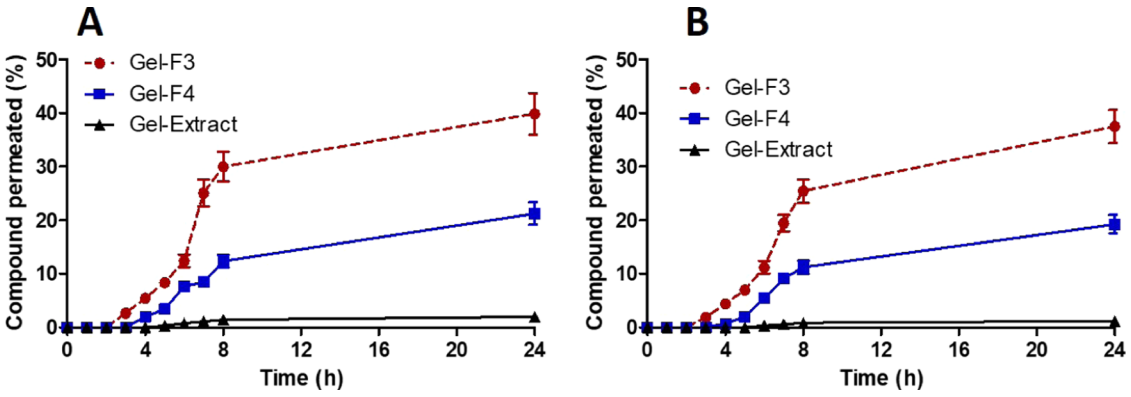

Figure 7. Ex vivo permeation profile of QU (A) and LU (B) from Gel-F3, Gel-F4, and Gel-Extract (means ± SD, n = 3).

did not differ significantly ($p > 0.05$), so from the results obtained, it can be concluded that the antioxidant effectiveness of SPE was not affected by the formulation produced.

Finally, the formulation was tested for the sun protecting factor (SPF) value. SPF is a quantitative measurement carried out to determine the effectiveness of a sunscreen formulation in its ability to protect and prevent skin damage. The in vitro SPF values were determined by UV spectrophotometry between the wavelengths of 290 and 320 nm to verify absorption in the UVB (290−320) regions. UVB is responsible for immediate damage, causing burns and skin cancer. Meanwhile, UVA radiation penetrates deeper and can damage the DNA, oxidize the lipids, and produce dangerous free radicals, which can cause inflammation, break the cellular communication, modify the gene expression in response to stress, and weaken the skin's immune response. But both radiations are linked to skin cancer.[69]

The US Food and Drug Administration (FDA) recommends that to help reduce the risk of sun damage, sunscreen products should have an SPF of 15 or higher.[69] In this study, it was found that the SPF value of the hydrogel formulation on SPE and SPE-loaded SLNs, F3, and F4 hydrogel were 16.54 ± 1.29, 15.69 ± 1.33, and 16.03 ± 1.41, respectively (Figure 8E). Based on statistical analysis, the formulations of SPE and SPE-loaded SLNs were not significantly different ($p > 0.05$). These results indicate that SPE incorporation into SLNs does not change SPE's ability to protect skin against UV light. All formulas have an SPF value > 15 in accordance with the recommendations from the FDA and the results obtained also indicate that this Safflower petal has high photoprotective properties.

https://doi.org/10.1021/acs.langmuir.2c02754
Langmuir XXXX, XXX, XXX−XXX

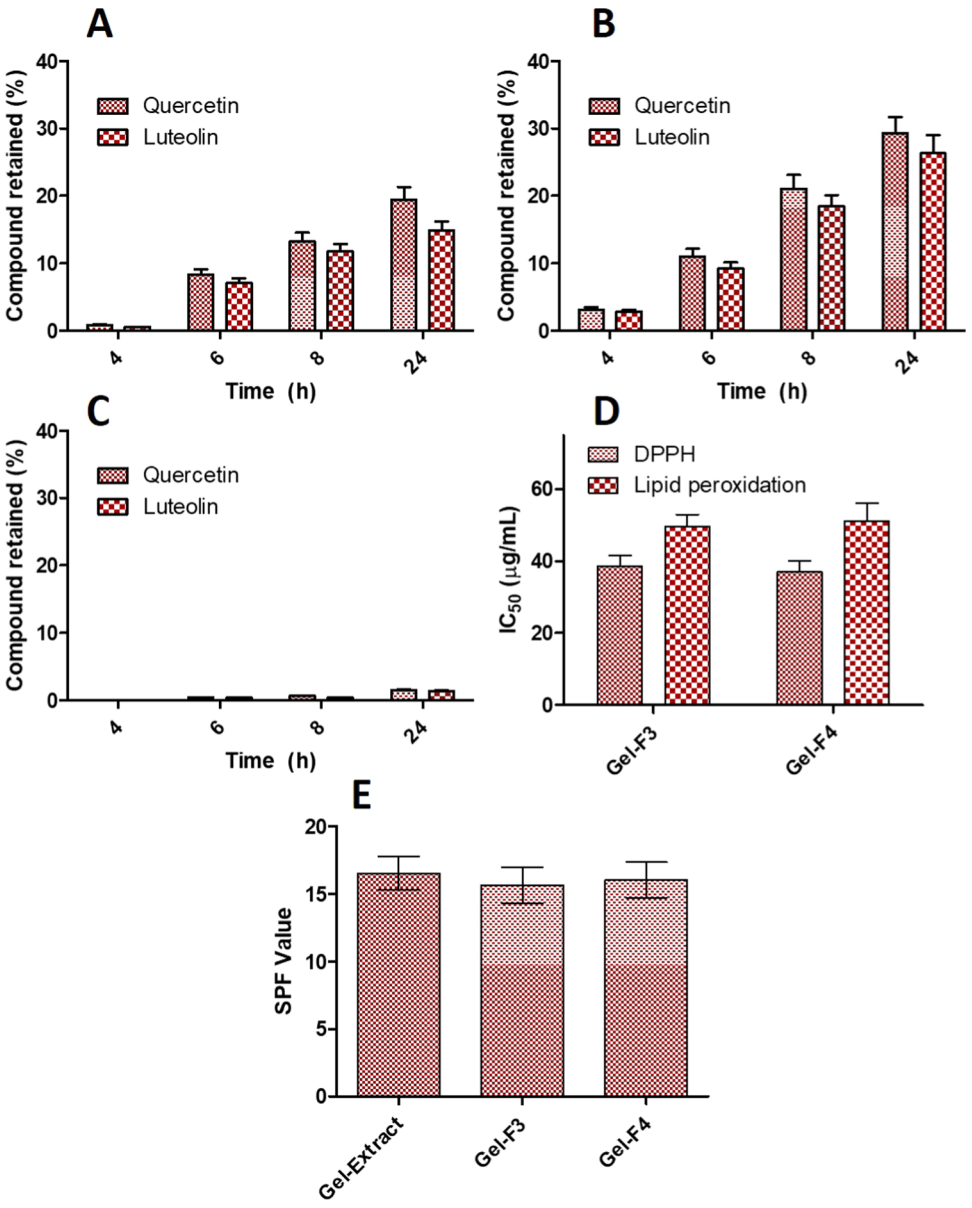

Figure 8. In vitro skin drug retention profiles of QU and LU after 24 h permeation study from Gel-F3 (A), Gel-F4 (B), Gel-Extract (C), antioxidant activity (IC50) against DPPH and lipid peroxidation of hydrogel (D), and SPF value (E) (means ± SD, n = 3).

Overall, the findings presented in this study indicate that the formulation of SPE-loaded SLNs leads to increased skin penetration and retention of the antioxidant substance of Safflower petals extract (SPE), QU, and LU. Then, after being formulated into the hydrogel, the SLNs also had no hemolytic effect and could adhere to the skin, which helped the user apply the gel and protect the skin against UV radiation. These results have provided new insights into the natural antioxidant compounds contained in safflower petals in developing topical drug delivery systems for these compounds. Moving forward, future research, including *in vivo* profile studies, must now be performed to investigate more about the antioxidant activity of SPE after providing this innovative approach to the experimental animals. In addition, it is also necessary to evaluate the safety and risk assessment of SPE-loaded SLN antioxidant products to prevent allergic reactions or significant biological effects when the product is applied topically.

4. CONCLUSIONS

In this work, the results of the determination of antioxidant compounds of SPE in ethanol extracts as well as their application in the form of SLN-based hydrogels were presented. Quercetin (QU) and luteolin (LU), the hydrophobic substances, were found to be the major chemical constituents isolated from SPE that is known to have antioxidant properties. Furthermore, the inclusion of SPE into SLN-based hydrogel formulations may favor the QU and LU solubility and penetration as well as its retention on the skin, which impacts the efficacy of photoprotective agents. The optimized F3 and F4 hydrogels tested were considered safe due to enhanced skin hydration and no hemolytic effect. Based on the results of antioxidant activity testing and SPF values, SPE-loaded SLN-based hydrogels show values that are in accordance with FDA recommendations and marked antioxidant activity in vitro, thus displaying enormous potential to be developed as a topical sunscreen to prevent symptoms

https://doi.org/10.1021/acs.langmuir.2c02754
Langmuir XXXX, XXX, XXX−XXX

associated with photoinduced skin aging. Furthermore, it is necessary to conduct *in vivo* method and risk assessment to the appropriate experimental animals to describe this typical antioxidant activity and safety of this innovative approach, thereby validating product performance and presenting a major limitation on the extent to which this material responds to the skin.

■ ASSOCIATED CONTENT

Supporting Information

The Supporting Information is available free of charge at https://pubs.acs.org/doi/10.1021/acs.langmuir.2c02754.

Optimization of safflower petals extraction method, yield of extraction, total phenolic and flavonoid contents determination, estimation of antioxidant activity using DPPH free-radical scavenging assay, and antioxidant activity using the lipid peroxidation method and HPLC assay of bioactive compounds in the extract (PDF)

■ AUTHOR INFORMATION

Corresponding Author

Andi Dian Permana − *Faculty of Pharmacy, Hasanuddin University, Makassar 90245, Indonesia;* orcid.org/0000-0003-2168-1688; Email: andi.dian.permana@farmasi.unhas.ac.id

Authors

Nuur Aanisah − *Department of Pharmacy, Faculty of Science, Tadulako University, Palu 94118, Indonesia*

Sulistiawati Sulistiawati − *Faculty of Pharmacy, Hasanuddin University, Makassar 90245, Indonesia*

Yulia Yusrini Djabir − *Faculty of Pharmacy, Hasanuddin University, Makassar 90245, Indonesia*

Rangga Meidianto Asri − *Faculty of Pharmacy, Hasanuddin University, Makassar 90245, Indonesia*

Sumarheni Sumarheni − *Faculty of Pharmacy, Hasanuddin University, Makassar 90245, Indonesia*

Lutfi Chabib − *Department of Pharmacy, Universitas Islam Indonesia, Yogyakarta 55584, Indonesia*

Hasyrul Hamzah − *Faculty of Pharmacy, Universitas Muhammadiyah Kalimantan Timur, Samarinda 75124, Indonesia*

Complete contact information is available at: https://pubs.acs.org/10.1021/acs.langmuir.2c02754

Author Contributions

The manuscript was written through contributions of all authors. All authors have given approval to the final version of the manuscript

Notes

The authors declare no competing financial interest.

■ ACKNOWLEDGMENTS

This work was supported by Penelitian Dasar Kompetitif Nasional (1268/UN4.22/PT.01.03/2022), Ministry of Education, Culture, Research and Technology of Republic of Indonesia.

■ REFERENCES

(1) Young, A. R.; Morgan, K. A.; Harrison, G. I.; Lawrence, K. P.; Petersen, B.; Wulf, H. C.; Philipsen, P. A. A Revised Action Spectrum for Vitamin D Synthesis by Suberythemal UV Radiation Exposure in Humans in Vivo. *Proc. Natl. Acad. Sci. U.S.A.* **2021**, *118*, No. e2015867118.

(2) Morita, A. Current Developments in Phototherapy for Psoriasis. *J. Dermatol.* **2018**, *45*, 287−292.

(3) Kohli, I.; Zubair, R.; Lyons, A. B.; Nahhas, A. F.; Braunberger, T. L.; Mokhtari, M.; Ruvolo, E.; Lim, H. W.; Hamzavi, I. H. Impact of Long-Wavelength Ultraviolet A1 and Visible Light on Light-Skinned Individuals. *Photochem. Photobiol.* **2019**, *95*, 1285−1287.

(4) Lim, H. W.; Kohli, I.; Ruvolo, E.; Kolbe, L.; Hamzavi, I. H. Impact of Visible Light on Skin Health: The Role of Antioxidants and Free Radical Quenchers in Skin Protection. *J. Am. Acad. Dermatol.* **2022**, *86*, S27−S37.

(5) Balupillai, A.; Nagarajan, R. P.; Ramasamy, K.; Govindasamy, K.; Muthusamy, G.*Caffeic Acid Prevents UVB Radiation Induced Photocarcinogenesis through Regulation of PTEN Signaling in Human Dermal Fibroblasts and Mouse Skin*; Elsevier Inc, 2018; Vol. *352*.

(6) Fukunaga, A.; Fukushima, S.; Iwata, H.; Nakahara, M.; Sasaki, R.; Baba, N.; Matsunaka, H.; Murakami, Y.; Furue, M.; Nishigori, C. Bioactive Substances in the Stratum Corneum of the Epidermis Found as Indicators of Skin Damage Due to Sun Exposure. *Photodermatol. Photoimmunol. Photomed.* **2022**, *38*, 241−249.

(7) Sample, A.; Zhao, B.; Qiang, L.; He, Y. Y. Adaptor Protein P62 Promotes Skin Tumor Growth and Metastasis and Is Induced by UVA Radiation. *J. Biol. Chem.* **2017**, *292*, 14786−14795.

(8) Plaza, M.; Pozzo, T.; Liu, J.; Gulshan Ara, K. Z.; Turner, C.; Nordberg Karlsson, E. Substituent Effects on in Vitro Antioxidizing Properties, Stability, and Solubility in Flavonoids. *J. Agric. Food Chem.* **2014**, *62*, 3321−3333.

(9) Roh, E.; Kim, J. E.; Kwon, J. Y.; Park, J. S.; Bode, A. M.; Dong, Z.; Lee, K. W. Molecular Mechanisms of Green Tea Polyphenols with Protective Effects against Skin Photoaging. *Crit. Rev. Food Sci. Nutr.* **2017**, *57*, 1631−1637.

(10) Yang, Q.; Yang, Z. F.; Liu, S. B.; Zhang, X. N.; Hou, Y.; Li, X. Q.; Wu, Y. M.; Wen, A. D.; Zhao, M. G. Neuroprotective Effects of Hydroxysafflor Yellow A against Excitotoxic Neuronal Death Partially through Down-Regulation of NR2B-Containing NMDA Receptors. *Neurochem. Res.* **2010**, *35*, 1353−1360.

(11) Orgah, J. O.; He, S.; Wang, Y.; Jiang, M.; Wang, Y.; Orgah, E. A.; Duan, Y.; Zhao, B.; Zhang, B.; Han, J.; Zhu, Y. Pharmacological Potential of the Combination of Salvia Miltiorrhiza (Danshen) and *Carthamus tinctorius* (Honghua) for Diabetes Mellitus and Its Cardiovascular Complications. *Pharmacol. Res.* **2020**, *153*, No. 104654.

(12) Yu, G.; Luo, Z.; Zhou, Y.; Zhang, L.; Wu, Y.; Ding, L.; Shi, Y. Uncovering the Pharmacological Mechanism of *Carthamus tinctorius* L. on Cardiovascular Disease by a Systems Pharmacology Approach. *Biomed. Pharmacother.* **2019**, *117*, No. 109094.

(13) Arpornsuwan, T.; Petvises, S.; Thim-Uam, A.; Boondech, A.; Roytrakul, S. Effects of *Carthamus tinctorius* L. Solvent Extracts on Anti-Proliferation of Human Colon Cancer (SW620 Cell Line) via Apoptosis and the Growth Promotion of Lymphocytes. *Songklanakarin J. Sci. Technol.* **2012**, *34*, 45−51.

(14) Loo, W. T. Y.; Cheung, M. N. B.; Chow, L. W. C. The Inhibitory Effect of a Herbal Formula Comprising Ginseng and *Carthamus tinctorius* on Breast Cancer. *Life Sci.* **2004**, *76*, 191−200.

(15) Wang, M.-n.; Cao, Y.-g.; Wei, Y.-x.; Ren, Y.-j.; Liu, Y.-l.; Chen, X.; He, C.; Zheng, X.-k.; Feng, W.-s. Saffloflavone, a New Flavonoid from the Flowers of *Carthamus tinctorius* L. and Its Cardioprotective Activity. *Nat. Prod. Res.* **2020**, *0*, 1−6.

(16) Asgarpanah, J.; Kazemivash, N. Phytochemistry, Pharmacology and Medicinal Properties of *Carthamus tinctorius* L. *Chin. J. Integr. Med.* **2013**, *19*, 153−159.

(17) Zhou, Y. Z.; Liu, X. X.; Zheng, X. H.; Zheng, J. Bin. Simultaneous Determination of Quercetin and Luteolin in Dried Flowers by Multivariate HPLC-ECD Calibration. *Chromatographia* **2007**, *66*, 635−637.

(18) Kurkin, V. A.; Kharisova, A. V. Flavonoids of *Carthamus tinctorius* Flowers. *Chem. Nat. Compd.* **2014**, *50*, 446−448.

(19) Censi, R.; Martena, V.; Hoti, E.; Malaj, L.; Di Martino, P. Permeation and Skin Retention of Quercetin from Microemulsions Containing Transcutol P. *Drug Dev. Ind. Pharm.* **2012**, *38*, 1128−1133.
(20) Kazmi, I.; Al-Abbasi, F. A.; Nadeem, M. S.; Altayb, H. N.; Alshehri, S.; Imam, S. S. Formulation, Optimization and Evaluation of Luteolin-Loaded Topical Nanoparticulate Delivery System for the Skin Cancer. *Pharmaceutics* **2021**, *13*, No. 1749.
(21) Permana, A. D.; Tekko, I. A.; McCarthy, H. O.; Donnelly, R. F. New HPLC−MS Method for Rapid and Simultaneous Quantification of Doxycycline, Diethylcarbamazine and Albendazole Metabolites in Rat Plasma and Organs after Concomitant Oral Administration. *J. Pharm. Biomed. Anal.* **2019**, *170*, 243−253.
(22) Altamimi, M. A.; Hussain, A.; Alshehri, S.; Imam, S. S.; Alnemer, U. A. Development and Evaluations of Transdermally Delivered Luteolin Loaded Cationic Nanoemulsion: In Vitro and Ex Vivo Evaluations. *Pharmaceutics* **2021**, *13*, No. 1218.
(23) Han, S. B.; Kwon, S. S.; Jeong, Y. M.; Yu, E. R.; Park, S. N. Physical Characterization and in Vitro Skin Permeation of Solid Lipid Nanoparticles for Transdermal Delivery of Quercetin. *Int. J. Cosmet. Sci.* **2014**, *36*, 588−597.
(24) Bose, S.; Du, Y.; Takhistov, P.; Michniak-Kohn, B. Formulation Optimization and Topical Delivery of Quercetin from Solid Lipid Based Nanosystems. *Int. J. Pharm.* **2013**, *441*, 56−66.
(25) Li, R.; Pu, C.; Sun, Y.; Sun, Q.; Tang, W. Interaction between Soybean Oleosome-Associated Proteins and Phospholipid Bilayer and Its Influence on Environmental Stability of Luteolin-Loaded Liposomes. *Food Hydrocolloids* **2022**, *130*, No. 107721.
(26) Chen-yu, G.; Yang, C. F.; Li, Q. L.; Tan, Q.; Xi, Y. W.; Liu, W. N.; Zhai, G. X. Development of a Quercetin-Loaded Nanostructured Lipid Carrier Formulation for Topical Delivery. *Int. J. Pharm.* **2012**, *430*, 292−298.
(27) Vicentini, F. T. M. C.; Simi, T. R. M.; Del Ciampo, J. O.; Wolga, N. O.; Pitol, D. L.; Iyomasa, M. M.; Bentley, M. V. L. B.; Fonseca, M. J. V. Quercetin in w/o Microemulsion: In Vitro and in Vivo Skin Penetration and Efficacy against UVB-Induced Skin Damages Evaluated in Vivo. *Eur. J. Pharm. Biopharm.* **2008**, *69*, 948−957.
(28) Sapino, S.; Ugazio, E.; Gastaldi, L.; Miletto, I.; Berlier, G.; Zonari, D.; Oliaro-Bosso, S. Mesoporous Silica as Topical Nanocarriers for Quercetin: Characterization and in Vitro Studies. *Eur. J. Pharm. Biopharm.* **2015**, *89*, 116−125.
(29) Chessa, M.; Caddeo, C.; Valenti, D.; Manconi, M.; Sinico, C.; Fadda, A. M. Effect of Penetration Enhancer Containing Vesicles on the Percutaneous Delivery of Quercetin through New Born Pig Skin. *Pharmaceutics* **2011**, *3*, 497−509.
(30) Netto MPharm, G.; Jose, J. Development, Characterization, and Evaluation of Sunscreen Cream Containing Solid Lipid Nanoparticles of Silymarin. *J. Cosmet. Dermatol.* **2018**, *17*, 1073−1083.
(31) Wissing, S. A.; Müller, R. H. A Novel Sunscreen System Based on Tocopherol Acetate Incorporated into Solid Lipid Nanoparticles. *Int. J. Cosmet. Sci.* **2001**, *23*, 233−243.
(32) Rodrigues, L. R.; Jose, J. Exploring the Photo Protective Potential of Solid Lipid Nanoparticle-Based Sunscreen Cream Containing *Aloe vera*. *Environ. Sci. Pollut. Res.* **2020**, *27*, 20876−20888.
(33) Manea, A. M.; Andronescu, C.; Meghea, A. Green Tea Extract Loaded into Solid Lipid Nanoparticles. *UPB Sci. Bull. Ser. B: Chem. Mater. Sci.* **2014**, *76*, 125−136.
(34) Khameneh, B.; Halimi, V.; Jaafari, M. R.; Golmohammadzadeh, S. Safranal-Loaded Solid Lipid Nanoparticles: Evaluation of Sunscreen and Moisturizing Potential for Topical Applications. *Iran. J. Basic Med. Sci.* **2015**, *18*, 58−63.
(35) zur Mühlen, A.; Schwarz, C.; Mehnert, W. Solid Lipid Nanoparticles (SLN) for Controlled Drug Delivery - Drug Release and Release Mechanism. *Eur. J. Pharm. Biopharm.* **1998**, *45*, 149−155.
(36) Wissing, S. A.; Lippacher, A.; Müller, R. H. Investigations on the Occlusive Properties of Solid Lipid Nanoparticles (SLN). *J. Cosmet. Sci.* **2001**, *52*, 313−324.
(37) Khalil, R. M.; Abd-Elbary, A.; Kassem, M. A.; Ghorab, M. M.; Basha, M. Nanostructured Lipid Carriers (NLCs) versus Solid Lipid Nanoparticles (SLNs) for Topical Delivery of Meloxicam. *Pharm. Dev. Technol.* **2014**, *19*, 304−314.
(38) Khalil, R. M.; El-bary, A. A.; Kassem, M. A.; Ghorab, M. M.; Ahmed, M. B. Solid Lipid Nanoparticles for Topical Delivery of Meloxicam: Development and In Vitro Characterization. *Eur. Sci. J.* **2013**, *4*, 24−26.
(39) Abdel-Salam, F. S.; Elkheshen, S. A.; Mahmoud, A. A.; Ammar, H. O. Diflucortolone Valerate Loaded Solid Lipid Nanoparticles as a Semisolid Topical Delivery System. *Bull. Fac. Pharm.* **2016**, *54*, 1−7.
(40) Tursilli, R.; Piel, G.; Delattre, L.; Scalia, S. Solid Lipid Microparticles Containing the Sunscreen Agent, Octyl-Dimethylaminobenzoate: Effect of the Vehicle. *Eur. J. Pharm. Biopharm.* **2007**, *66*, 483−487.
(41) Lu, Y.; Liu, M.; Cao, Y.; Yin, J.; Zhou, H.; Yu, W.; Liu, H.; Wang, J.; Huang, C.; Ma, P.; Que, S.; Gong, C.; Zhao, G. Hydrogel Sunscreen Based on Yeast /Gelatin Demonstrates Excellent UV-Shielding and Skin Protection Performance. *Colloids Surf., B* **2021**, *205*, No. 111885.
(42) Wang, R.; Wang, X.; Zhan, Y.; Xu, Z.; Xu, Z.; Feng, X.; Li, S.; Xu, H. A Dual Network Hydrogel Sunscreen Based on Poly-γ-Glutamic Acid/Tannic Acid Demonstrates Excellent Anti-UV, Self-Recovery, and Skin-Integration Capacities. *ACS Appl. Mater. Interfaces* **2019**, *11*, 37502−37512.
(43) Gwak, M. A.; Hong, B. M.; Park, W. H. Hyaluronic Acid/Tannic Acid Hydrogel Sunscreen with Excellent Anti-UV, Antioxidant, and Cooling Effects. *Int. J. Biol. Macromol.* **2021**, *191*, 918−924.
(44) Tan, F.; Cui, H.; Bai, C.; Qing, C.; Xu, L.; Han, J. Preparation, Optimization, and Transcorneal Permeability Study of Lutein-Loaded Solid Lipid Nanoparticles. *J. Drug Delivery Sci. Technol.* **2021**, *62*, No. 102362.
(45) Patil, J.; Rajput, R.; Nemade, R.; Naik, J. Preparation and Characterization of Artemether Loaded Solid Lipid Nanoparticles: A 32 Factorial Design Approach. *Mater. Technol.* **2020**, *35*, 719−726.
(46) Priyanka, K.; Sahu, P. L.; Singh, S. Optimization of Processing Parameters for the Development of Ficus Religiosa L. Extract Loaded Solid Lipid Nanoparticles Using Central Composite Design and Evaluation of Antidiabetic Efficacy. *J. Drug Delivery Sci. Technol.* **2018**, *43*, 94−102.
(47) Mir, M.; Permana, A. D.; Tekko, I. A.; McCarthy, H. O.; Ahmed, N.; Rehman, A. Ur.; Donnelly, R. F. Microneedle Liquid Injection System Assisted Delivery of Infection Responsive Nanoparticles: A Promising Approach for Enhanced Site-Specific Delivery of Carvacrol against Polymicrobial Biofilms-Infected Wounds. *Int. J. Pharm.* **2020**, *587*, No. 119643.
(48) Enggi, C. K.; Isa, H. T.; Sulistiawati, S.; Ardika, K. A. R.; Wijaya, S.; Asri, R. M.; Mardikasari, S. A.; Donnelly, R. F.; Permana, A. D. Development of Thermosensitive and Mucoadhesive Gels of Cabotegravir for Enhanced Permeation and Retention Profiles in Vaginal Tissue: A Proof of Concept Study. *Int. J. Pharm.* **2021**, *609*, No. 121182.
(49) Khurana, S.; Bedi, P. M. S.; Jain, N. K. Preparation and Evaluation of Solid Lipid Nanoparticles Based Nanogel for Dermal Delivery of Meloxicam. *Chem. Phys. Lipids* **2013**, *175*−*176*, 65−72.
(50) Permana, A. D.; Tekko, I. A.; McCrudden, M. T. C.; Anjani, Q. K.; Ramadon, D.; McCarthy, H. O.; Donnelly, R. F. Solid Lipid Nanoparticle-Based Dissolving Microneedles: A Promising Intradermal Lymph Targeting Drug Delivery System with Potential for Enhanced Treatment of Lymphatic Filariasis. *J. Control. Release* **2019**, *316*, 34−52.
(51) Rostamkalaei, S. S.; Akbari, J.; Saeedi, M.; Morteza-Semnani, K.; Nokhodchi, A. Topical Gel of Metformin Solid Lipid Nanoparticles: A Hopeful Promise as a Dermal Delivery System. *Colloids Surf., B* **2019**, *175*, 150−157.
(52) Vaghasiya, H.; Kumar, A.; Sawant, K. Development of Solid Lipid Nanoparticles Based Controlled Release System for Topical Delivery of Terbinafine Hydrochloride. *Eur. J. Pharm. Sci.* **2013**, *49*, 311−322.

https://doi.org/10.1021/acs.langmuir.2c02754
Langmuir XXXX, XXX, XXX−XXX

(53) Zhu, R. R.; Qin, L. L.; Wang, M.; Wu, S. M.; Wang, S. L.; Zhang, R.; Liu, Z. X.; Sun, X. Y.; Yao, S. D. Preparation, Characterization, and Anti-Tumor Property of Podophyllotoxin-Loaded Solid Lipid Nanoparticles. *Nanotechnology* **2009**, *20*, No. 055702.
(54) Das, S.; Ng, W. K.; Kanaujia, P.; Kim, S.; Tan, R. B. H. Formulation Design, Preparation and Physicochemical Characterizations of Solid Lipid Nanoparticles Containing a Hydrophobic Drug: Effects of Process Variables. *Colloids Surf., B* **2011**, *88*, 483−489.
(55) De Souza, A. L. R.; Andreani, T.; Nunes, F. M.; Cassimiro, D. L.; De Almeida, A. E.; Ribeiro, C. A.; Sarmento, V. H. V.; Gremião, M. P. D.; Silva, A. M.; Souto, E. B. Loading of Praziquantel in the Crystal Lattice of Solid Lipid Nanoparticles: Studies by DSC and SAXS. *J. Therm. Anal. Calorim.* **2012**, *108*, 353−360.
(56) Üner, M.; Karaman, E. F.; Aydoğmuş, Z. Solid Lipid Nanoparticles and Nanostructured Lipid Carriers of Loratadine for Topical Application: Physicochemical Stability and Drug Penetration through Rat Skin. *Trop. J. Pharm. Res.* **2014**, *13*, 653−660.
(57) Perkin, A. G.; Horsfall, L. H. CXXVI.—Luteolin. Part III. *J. Chem. Soc. Trans.* **1900**, *77*, 1314−1324.
(58) Ice, C. H.; Wender, S. H. Quercetin and Its Glycosides in Leaves of Vaccinium Myrtillus. *J. Am. Chem. Soc.* **1953**, *75*, 50−52.
(59) Sadegh Malvajerd, S.; Azadi, A.; Izadi, Z.; Kurd, M.; Dara, T.; Dibaei, M.; Sharif Zadeh, M.; Akbari Javar, H.; Hamidi, M. Brain Delivery of Curcumin Using Solid Lipid Nanoparticles and Nanostructured Lipid Carriers: Preparation, Optimization, and Pharmacokinetic Evaluation. *ACS Chem. Neurosci.* **2019**, *10*, 728−739.
(60) Sharma, M.; Sharma, R.; Jain, D. K.; Saraf, A. Enhancement of Oral Bioavailability of Poorly Water Soluble Carvedilol by Chitosan Nanoparticles: Optimization and Pharmacokinetic Study. *Int. J. Biol. Macromol.* **2019**, *135*, 246−260.
(61) Bolla, P. K.; Kalhapure, R. S.; Rodriguez, V. A.; Ramos, D. V.; Dahl, A.; Renukuntla, J. Preparation of Solid Lipid Nanoparticles of Furosemide-Silver Complex and Evaluation of Antibacterial Activity. *J. Drug Delivery Sci. Technol.* **2019**, *49*, 6−13.
(62) Zhou, H. Y.; Zhang, Y. P.; Zhang, W. F.; Chen, X. G. Biocompatibility and Characteristics of Injectable Chitosan-Based Thermosensitive Hydrogel for Drug Delivery. *Carbohydr. Polym.* **2011**, *83*, 1643−1651.
(63) Ramasamy, T.; Khandasami, U. S.; Ruttala, H.; Shanmugam, S. Development of Solid Lipid Nanoparticles Enriched Hydrogels for Topical Delivery of Anti-Fungal Agent. *Macromol. Res.* **2012**, *20*, 682−692.
(64) Kelidari, H. R.; Saeedi, M.; Akbari, J.; Morteza-Semnani, K.; Gill, P.; Valizadeh, H.; Nokhodchi, A. Formulation Optimization and in Vitro Skin Penetration of Spironolactone Loaded Solid Lipid Nanoparticles. *Colloids Surf., B* **2015**, *128*, 473−479.
(65) Lademann, J.; Richter, H.; Schanzer, S.; Knorr, F.; Meinke, M.; Sterry, W.; Patzelt, A. Penetration and Storage of Particles in Human Skin: Perspectives and Safety Aspects. *Eur. J. Pharm. Biopharm.* **2011**, *77*, 465−468.
(66) Betageri, G. V.; Deshmukh, D. V.; Gupta, R. B. Oral Sustained-Release Bioadhesive Tablet Formulation of Didanosine. *Drug Dev. Ind. Pharm.* **2001**, *27*, 129−136.
(67) Calixto, G.; Yoshii, A. C.; Rocha E Silva, H.; Stringhetti Ferreira Cury, B.; Chorilli, M. Polyacrylic Acid Polymers Hydrogels Intended to Topical Drug Delivery: Preparation and Characterization. *Pharm. Dev. Technol.* **2015**, *20*, 490−496.
(68) Dupont, E.; Gomez, J.; Bilodeau, D. Beyond UV Radiation: A Skin under Challenge. *Int. J. Cosmet. Sci.* **2013**, *35*, 224−232.
(69) FDA. Tips to Stay Safe in the Sun: From Sunscreen to Sunglasses https://www.fda.gov/consumers/consumer-updates/tips-stay-safe-sun-sunscreen-sunglasses (accessed Aug 11, 2022).

https://doi.org/10.1021/acs.langmuir.2c02754
Langmuir XXXX, XXX, XXX−XXX